

# A New Chiral Beam Element for Modelling Chiral Honeycombs

Lu X<sup>1\*</sup>, Chen BY<sup>2</sup>, Tan VBC<sup>1</sup> and Tay TE<sup>1</sup>

<sup>1</sup>Department of Mechanical Engineering, National University of Singapore, Singapore

<sup>2</sup>Department of Technology and Research, Institute of High Performance Computing, Singapore

## Abstract

Chiral honeycombs which exhibit auxetic behaviors (negative Poisson's ratios) have attracted much research interest due to their novel mechanical properties. They are broadly used in designing new functional structures, such as energy absorption and noise mitigation materials. To analyze the behaviors of these materials, finite element models are generally adopted, which may require much time and labor to construct and implement. To simplify the numerical modelling, a novel Chiral Beam Element for finite element simulation is proposed in this paper. Both static and dynamic analyses are conducted and the numerical expense, i.e., the modelling procedures and the computational time, is reduced significantly when compared to traditional finite element models.

**Keywords:** Chiral honeycombs; Meta-materials; Negative Poisson's ratio; Finite element method; Elastic constants; Dynamic analysis

## Introduction

As shown in Figure 1a, the fundamental building block of chiral honeycombs can be constructed by attaching the circular nodes on different sides of the ligament. With three, four or six ligaments connected to the central node, the trichiral, tetrachiral or hexachiral honeycombs may be generated, respectively (Figures 1b-1d) [1]. Chiral honeycombs are found to exhibit auxetic properties and undergo lateral extension when stretched [2,3]. The so-called negative Poisson's ratio as well as other elastic properties can be obtained by investigating the constitutive relations [4-7]. Aimed at different applications, these chiral honeycombs can also be adopted to design new structures and materials [8-10]. For example, incorporated with local resonators or discrete masses, the chiral honeycombs may be employed for the purpose of vibration control and wave mitigation [11-14].

To study these static and dynamic properties of chiral honeycombs, representative volume element (RVE) together with periodic boundary conditions (PBC) are usually employed in both theoretical and finite element (FE) models [15-19]. However, if finite geometric configurations, irregular loadings or disordered structures are considered, RVEs cannot be used and full FE models are required [11,12,20]. In this case, it will be tedious to build up these FE models and time-consuming to implement the numerical simulations.

In order to simplify the FE models of these chiral honeycombs, a new Chiral Beam Element (CBE) based on the fundamental building block (Figure 1a) is proposed in this paper. Given the properly defined stiffness and mass matrices, this user-defined CBE can be applied to static and dynamic FE simulations. As will be shown afterwards, both ordered and disordered chiral honeycombs can be dealt with easily and more significantly, the time and labor is saved to a great extent by adopting the CBE in FE modelling.

## Chiral Beam Element (CBE)

As shown in Figure 1, arranged in different manners, the fundamental micro structures (Figure 1a) can be utilized to build up various types of chiral honeycomb structures. Following the same concept, if an equivalent FE for this micro structure can be established, the modelling procedure will become much more straightforward. In this section, the construction of the user-defined CBE from the micro

structure will be presented and the stiffness and mass matrices are derived respectively.

## Stiffness matrix of the CBE

As shown in Figure 2, the user-defined CBE is derived from the fundamental micro structure. The nodes may be hollow or solid in the real cases, but in this paper, they are assumed rigid while only the ligament (treated as a slender beam) is considered as deformable [1,14,16,21]. With this assumption, the nodes may be replaced by the material points ( $B$  and  $D$  in Figure 2) whose translational and rotational motions are related to the elastic ligament. Then, the micro structure can be directly represented by a CBE that geometrically shares the same points  $B$  and  $D$ . The CBE will possess two element nodes and three degrees of freedom (DoF) for each node,

$$\{u_B \ v_B \ \phi_B \ u_D \ v_D \ \phi_D\}^T, \{F_{xB} \ F_{yB} \ m_B \ F_{xD} \ F_{yD} \ m_D\}^T \quad (1)$$

Where, as shown in Figure 2,  $u_i$  and  $v_i$  are the translational displacements while  $\phi_i$  is the rotational displacement;  $F_{yi}$  and  $F_{xi}$  are the axial forces corresponding to the translational displacements;  $m_i$  is the moment corresponding to the rotational displacement. ( $i=B$  and  $C$ , referring to the two element nodes).

The CBE defined here is similar to the general beam element in terms of the element configuration and DoF. However, the stiffness matrix which relates the nodal displacements and forces is different. In order to faithfully represent the fundamental micro structure, the intrinsic properties of the structure, such as the coupling motions between the nodes and ligament, must be taken into consideration when constructing this CBE. As shown in the following sections, this relationship can be obtained by investigating the kinematic and mechanical connections between the rigid nodes and the elastic ligament.

**\*Corresponding author:** Lu X, Department of Mechanical Engineering, National University of Singapore - 117576, Singapore, Tel: +65 9120 0392; E-mail: xinlu@u.nus.edu

**Received** December 16, 2016; **Accepted** January 17, 2017; **Published** January 20, 2017

**Citation:** Lu X, Chen BY, Tan VBC, Tay TE (2017) A New Chiral Beam Element for Modelling Chiral Honeycombs. J Appl Mech Eng 6: 249. doi: 10.4172/2168-9873.1000249

**Copyright:** © 2017 Lu X, et al. This is an open-access article distributed under the terms of the Creative Commons Attribution License, which permits unrestricted use, distribution, and reproduction in any medium, provided the original author and source are credited.

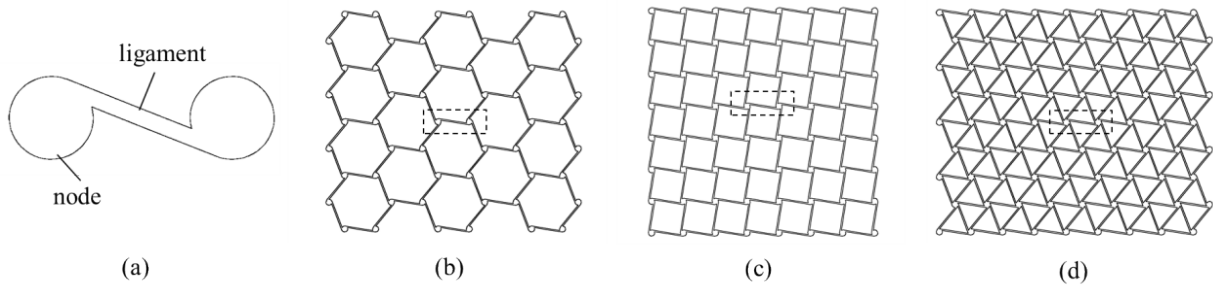


**Figure 1:** Chiral honeycombs of different types: (a) fundamental building block (micro structure); (b) trichiral honeycomb (120° rotational symmetry); (c) tetrachiral honeycomb (90° rotational symmetry); (d) hexachiral honeycomb (60° rotational symmetry).

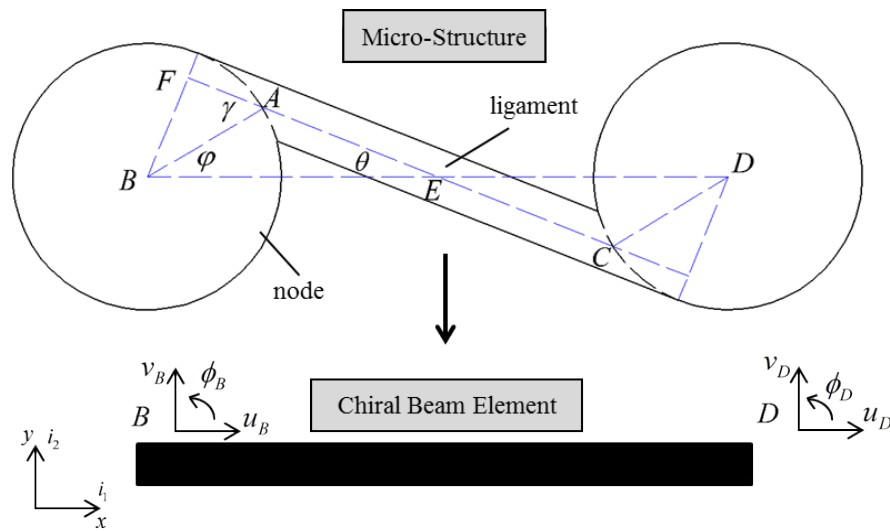


**Figure 2:** From micro structure to chiral beam element: geometric parameters and the degrees of freedom.

**The geometric relationship:** From Figure 2, the radius of the circular node is  $r$  and the thickness of the ligament is  $t$ ,

$$\overline{AB} = r, \quad \overline{BF} = r - 0.5t \quad (2)$$

The length of the ligament is  $L$ , so  $EF$  is half of this length,

$$\overline{EF} = 0.5L \quad (3)$$

The distance between  $B$  and  $D$  is the length of the user-defined element, defined as  $L_E$ ,

$$\overline{BD} = L_E \quad (4)$$

The trigonometric relations according to Fig. 2 are,

$$\sin \gamma = \frac{2r-t}{2r}, \quad \cos \gamma = \sqrt{1 - \sin^2 \gamma} \quad (5)$$

$$\sin \theta = \frac{2r-t}{L_E}, \quad \cos \theta = \frac{L}{L_E} \quad (6)$$

Since  $\varphi = \gamma - \theta$ , applying the summation and difference rule, we will have,

$$\cos \varphi = \cos(\gamma - \theta) = \cos \gamma \cos \theta + \sin \gamma \sin \theta \quad (7)$$

$$\sin \varphi = \sin(\gamma - \theta) = \sin \gamma \cos \theta - \cos \gamma \sin \theta \quad (8)$$

Due to the geometric constraints, the effective length for the elastic

ligament should be considered [1,22]. As shown in Figure 2,  $AC$  is assumed to be the effective beam and the length is,

$$l = \overline{AC} = 2(\overline{FE} - \overline{AE}) = L - 2r \cos \varphi \quad (9)$$

**Rigid node transformation:** The node is assumed to be rigid and as shown in Figure 3, the kinematic relation between the center point  $B$  and the circumferential point  $A$  is given by the following [16],

$$\mathbf{OA} = \mathbf{OB} + \mathbf{BA} = \mathbf{OB} + r(\cos \varphi \mathbf{i}_1 + \sin \varphi \mathbf{i}_2) \quad (10)$$

After translation and rotation of the node,

$$\mathbf{OA}' = \mathbf{OB}' + \mathbf{B}'\mathbf{A}' = \mathbf{OB} + (u_B \mathbf{i}_1 + v_B \mathbf{i}_2) + r(\cos(\varphi + \phi) \mathbf{i}_1 + \sin(\varphi + \phi) \mathbf{i}_2) \quad (11)$$

Assuming small rotation of the node, we obtain the displacement of  $A$ ,

$$\begin{aligned} \mathbf{u}_A &= \mathbf{OA}' - \mathbf{OA} \\ &= (u_B \mathbf{i}_1 + v_B \mathbf{i}_2) + r[(\cos(\varphi + \phi) - \cos \varphi) \mathbf{i}_1 + (\sin(\varphi + \phi) - \sin \varphi) \mathbf{i}_2] \\ &\approx \mathbf{u}_B + r[-\phi \sin \varphi \mathbf{i}_1 + \phi \cos \varphi \mathbf{i}_2] \end{aligned} \quad (12)$$

The rotation is same for point  $A$  and point  $B$  and thus we have,

$$\mathbf{U}_A = \begin{bmatrix} u_A \\ v_A \\ \phi_A \end{bmatrix} = \begin{bmatrix} 1 & 0 & -r \sin \varphi \\ 0 & 1 & r \cos \varphi \\ 0 & 0 & 1 \end{bmatrix} \begin{bmatrix} u_B \\ v_B \\ \phi_B \end{bmatrix} = \overline{\mathbf{T}}(\varphi) \mathbf{U}_B \quad (13)$$

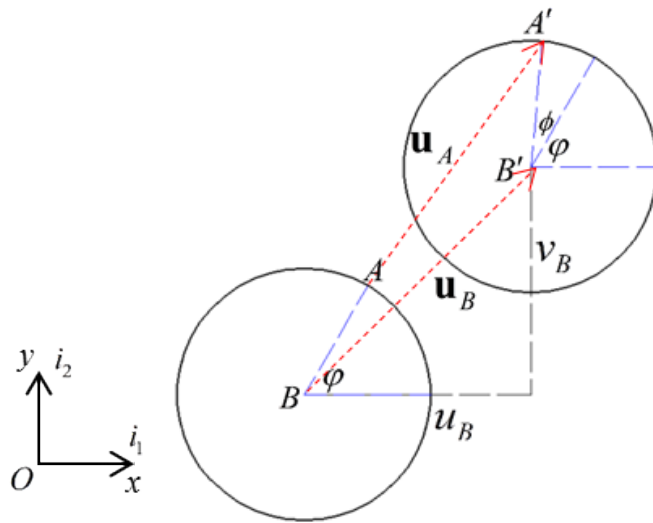


Figure 3: Rigid node transformation: displacements of point A on the circumference are determined by the node B through rigid translation and rotation.

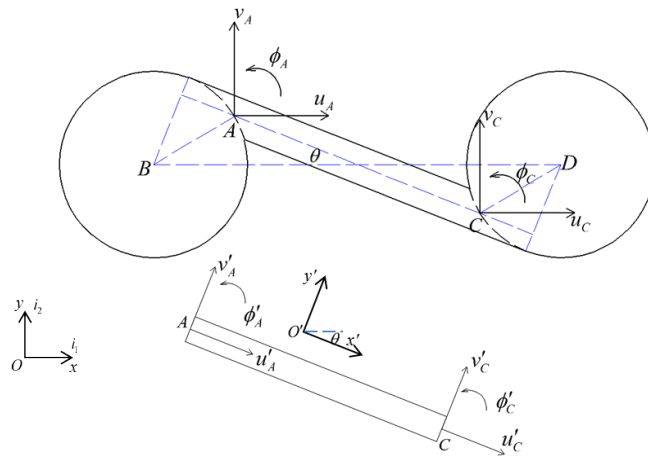


Figure 4: Global coordinates Oxy to local coordinates O'x'y': the displacements of point A and C in global coordinates are transformed to the local coordinates aligned to the ligament.

Consider both nodes of this element (Figure 2), the nodal displacements of CBE,  $U_B$  and  $U_A$ , are related to the ligament displacements,  $U_A$  and  $U_C$ ,

$$\begin{bmatrix} U_A \\ U_C \end{bmatrix} = \begin{bmatrix} \bar{T}(\varphi) & \mathbf{0} \\ \mathbf{0} & \bar{T}(\pi + \varphi) \end{bmatrix} \begin{bmatrix} U_B \\ U_D \end{bmatrix} \quad (14)$$

**Global displacements to local displacements:** As shown in Figure 4, the global displacements at point A are transformed to the local coordinates through rotation transformation,

$$U'_A = \bar{R}(\theta)U_A \quad (15)$$

$$\bar{R}(\theta) = \begin{bmatrix} \cos \theta & -\sin \theta & 0 \\ \sin \theta & \cos \theta & 0 \\ 0 & 0 & 1 \end{bmatrix} \quad (16)$$

Consider both nodes of the ligament,

$$\begin{bmatrix} U'_A \\ U'_C \end{bmatrix} = \begin{bmatrix} \bar{R}(\theta) & \mathbf{0} \\ \mathbf{0} & \bar{R}(\theta) \end{bmatrix} \begin{bmatrix} U_A \\ U_C \end{bmatrix} \quad (17)$$

**Force transformations:** The ligament AC is treated as a slender beam. Given the displacements, the reaction forces can be derived. These forces obtained from beam theory are located at points A and C in local coordinates. They are firstly translated to the element nodes B and D (Figure 5a), and then rotated to global coordinates (Figure 5b). The forces shown in Figure 5b are the nodal forces of the CBE.

Firstly, translate the forces from points A, C to points B, D under local coordinates,

$$\mathbf{F}'_B = \begin{bmatrix} F'_{xB} \\ F'_{yB} \\ m'_B \end{bmatrix} = \begin{bmatrix} 1 & 0 & 0 \\ 0 & 1 & 0 \\ -(r-t)/2 & r \cos \gamma & 1 \end{bmatrix} \begin{bmatrix} F'_{xA} \\ F'_{yA} \\ m'_A \end{bmatrix} = \bar{Q}_1 \mathbf{F}'_A \quad (18)$$

$$\mathbf{F}'_D = \begin{bmatrix} F'_{xD} \\ F'_{yD} \\ m'_D \end{bmatrix} = \begin{bmatrix} 1 & 0 & 0 \\ 0 & 1 & 0 \\ (r-t)/2 & -r \cos \gamma & 1 \end{bmatrix} \begin{bmatrix} F'_{xC} \\ F'_{yC} \\ m'_C \end{bmatrix} = \bar{Q}_2 \mathbf{F}'_C \quad (19)$$

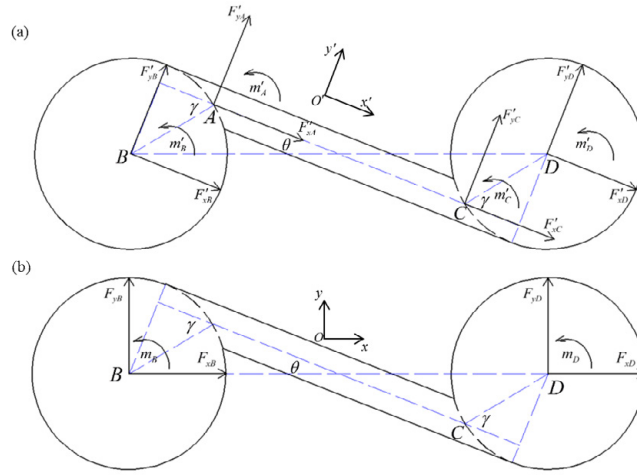


Figure 5: Force transformations: (a) translation from points A and C to points B and D; (b) rotation from local coordinates to the global coordinates.

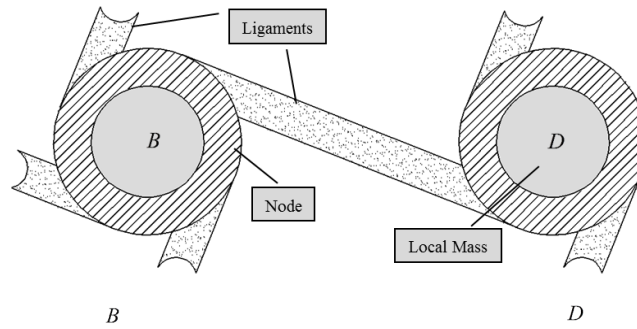


Figure 6: Mass distribution of the micro structure.

$$\begin{bmatrix} \mathbf{F}'_B \\ \mathbf{F}'_D \end{bmatrix} = \begin{bmatrix} \bar{\mathbf{Q}}_1 & \mathbf{0} \\ \mathbf{0} & \bar{\mathbf{Q}}_2 \end{bmatrix} \begin{bmatrix} \mathbf{F}'_A \\ \mathbf{F}'_C \end{bmatrix} \quad (20)$$

Then, the forces are rotated to the global coordinates,

$$\begin{bmatrix} \mathbf{F}_B \\ \mathbf{F}_D \end{bmatrix} = \begin{bmatrix} \bar{\mathbf{R}}(-\theta) & \mathbf{0} \\ \mathbf{0} & \bar{\mathbf{R}}(-\theta) \end{bmatrix} \begin{bmatrix} \mathbf{F}'_B \\ \mathbf{F}'_D \end{bmatrix} \quad (21)$$

**Assembly:** The relationship between the forces and displacement at the points A and C can be derived through Euler beam theory,

$$\begin{bmatrix} \mathbf{F}'_A \\ \mathbf{F}'_C \end{bmatrix} = \bar{\mathbf{K}}_b \begin{bmatrix} \mathbf{U}'_A \\ \mathbf{U}'_C \end{bmatrix} \quad (22)$$

where, \$\bar{\mathbf{K}}\_b\$ is the stiffness matrix of the slender beam,

$$\bar{\mathbf{K}}_b = \begin{bmatrix} EA/L & 0 & 0 & -EA/L & 0 & 0 \\ 12EI/l^3 & 6EI/l^2 & 0 & -12EI/l^3 & 6EI/l^2 & 0 \\ s & 4EI/l & 0 & -6EI/l^2 & 2EI/l & 0 \\ y & EA/L & 0 & 0 & 0 & 0 \\ m & 0 & 0 & 12EI/l^3 & -6EI/l^2 & 4EI/l \end{bmatrix} \quad (23)$$

With all the transformation mentioned above, Eq. (14-15, 17, 20-21), the forces and displacements of nodes B and D can be related,

$$\begin{bmatrix} \mathbf{F}_B \\ \mathbf{F}_D \end{bmatrix} = \begin{bmatrix} \bar{\mathbf{R}}(-\theta) & \mathbf{0} \\ \mathbf{0} & \bar{\mathbf{R}}(-\theta) \end{bmatrix} \begin{bmatrix} \bar{\mathbf{Q}}_1 & \mathbf{0} \\ \mathbf{0} & \bar{\mathbf{Q}}_2 \end{bmatrix} \bar{\mathbf{K}}_b \begin{bmatrix} \bar{\mathbf{R}}(\theta) & \mathbf{0} \\ \mathbf{0} & \bar{\mathbf{R}}(\theta) \end{bmatrix} \begin{bmatrix} \bar{\mathbf{T}}(\varphi) & \mathbf{0} \\ \mathbf{0} & \bar{\mathbf{T}}(\pi+\varphi) \end{bmatrix} \begin{bmatrix} \mathbf{U}_B \\ \mathbf{U}_D \end{bmatrix} \quad (24)$$

$$\begin{bmatrix} \mathbf{F}_B \\ \mathbf{F}_D \end{bmatrix} = \bar{\mathbf{K}}_N \begin{bmatrix} \mathbf{U}_B \\ \mathbf{U}_D \end{bmatrix} \quad (25)$$

where, \$\bar{\mathbf{K}}\_N\$ is the stiffness matrix for the user-defined CBE.

### Mass matrix of CBE

The mass matrix of the CBE is defined in this section. As shown in Figure 6, the total mass of the micro structure consists of the mass of the ligament (\$M\_{lig}\$), the mass of hollow node (\$M\_{node}\$) and the local mass (\$M\_{mass}\$). The ligament only belongs to the CBE itself while the node and the local masses are shared by the adjacent elements. As shown in Figure 6, the node B is shared by 4 neighboring elements while node D is shared by 3 elements. Let \$n\_1\$ and \$n\_2\$ denote the number of elements that share node B and node D respectively and we will have \$n\_1=4\$ and \$n\_2=3\$. As shown below, the global connectivity represented by \$n\_1\$ and \$n\_2\$ will be considered when forming element mass matrix [22].

First of all, the mass of the ligament is considered. Since the ligament is treated as a slender beam, the mass matrix can be given as [23],

$$\bar{\mathbf{M}}_{lig} = \rho A \int (\mathbf{N})^T (\mathbf{N}) dl = \frac{M_{lig}}{420} \begin{bmatrix} 140 & 0 & 0 & 70 & 0 & 0 \\ 0 & 156 & 22L_E & 0 & 54 & -13L_E \\ 0 & 22L_E & 4L_E^2 & 0 & 13L_E & -3L_E^2 \\ 70 & 0 & 0 & 140 & 0 & 0 \\ 0 & 54 & 13L_E & 0 & 156 & -22L_E \\ 0 & -13L_E & -3L_E^2 & 0 & -22L_E & 4L_E^2 \end{bmatrix} \quad (26)$$

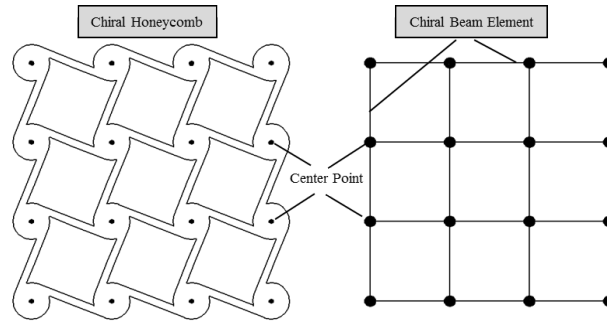


Figure 7: CBE modelling chiral honeycomb: connect the center points of the nodes in the micro structures with CBEs.

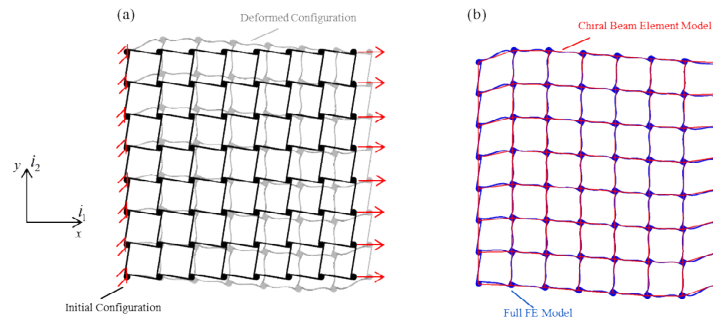


Figure 8: Tetrachiral honeycomb (a) initial and deformed configurations with full FE; (b) superposition of the deformed shapes of full FE model and CBE model.

Then, taking the mass of node and local mass into account and considering the connection effect, the mass matrix for the remaining parts, the nodes and internal masses, can be obtained as,

$$\bar{\mathbf{M}} = \begin{bmatrix} a & 0 & \dots & \dots & 0 \\ 0 & a & & & \\ \dots & \dots & b & & \\ \dots & \dots & \dots & c & \\ \dots & \dots & \dots & \dots & c & 0 \\ 0 & \dots & \dots & \dots & 0 & d \end{bmatrix} \quad (27)$$

with,

$$a = \frac{(M_{mass} + M_{node})}{n_1}, b = \frac{(J_{mass} + J_{node})}{n_1}, c = \frac{(M_{mass} + M_{node})}{n_2}, d = \frac{(J_{mass} + J_{node})}{n_2} \quad (28)$$

Where,  $J_{mass}$  and  $J_{node}$  are the moments of inertia for the local masses and the hollow nodes.

Combining Eq. (26) and Eq. (27), the full mass matrix for the CBE is established,

$$\bar{\mathbf{M}} = \bar{\mathbf{M}}' + \bar{\mathbf{M}}_{lig} \quad (29)$$

Eq. (25) and Eq. (29) define the stiffness and mass matrices of the CBE and with these matrices, the CBE can be constructed and employed in FE modelling

## Numerical Examples

The chiral honeycombs can be represented and modeled easily with the CBE defined in section 2. As shown in Figure 7, the center points of the micro structures are consistent with the elemental nodes of CBEs. According to the real structure of interest, connect these center points with the CBEs and the equivalent CBE model is obtained.

In this section, the CBE is employed to simulate honeycombs of different types (ordered and disordered) for both static and dynamic analyses. Numerical analyses are performed using Abaqus software package (Version 6.14). The CBE models are constructed using the user element defined in Abaqus UEL subroutine while two-dimensional solid elements (CPS4R) are employed to build up the full FE models for comparison. The performance of the CBE is verified through several examples shown below.

### Static analyses

As examples, CBE with  $L=100 \text{ mm}$ ,  $t=4 \text{ mm}$  and  $r=10 \text{ mm}$  are adopted. The Young's modulus and Poisson's ratio are set to be 1600 Mpa and 0.36. Tetrachiral, trichiral and disordered honeycombs are studied. Setting the results from full FE models as the benchmarks, the efficiency and global accuracy of the CBE models can be obtained.

### Tetrachiral Honeycomb

As shown in Figure 8, both full FE and CBE are used to simulate this tetrachiral honeycomb. The left edge of the structure is fixed and uniaxial tension is conducted by imposing axial displacements on the right edge ( $U1=10 \text{ mm}$  and  $U2=0 \text{ mm}$ , along x and y directions respectively). As can be seen from Figure 8b, the CBE model coincides with the full FE model in terms of the deformed shapes and it should be noted the curved and irregular shapes can be captured accurately.

As shown in Table 1, the displacements of the right edge ( $U1$  and  $U2$ ) are prescribed while the reaction forces on the right edge,  $RF1$  along x direction and  $RF2$  along y direction, are obtained from numerical models. If the full FE model is regarded as a reference, the relative errors of the reaction forces between full FE and CBE models can be calculated by,

Parameter	U1 (mm)	U2 (mm)	RF1 (N)	RF2 (N)	NOE	Time (s)
Full-FE	10	0	115.2506	-9.13875	287591	158.7
CBE	10	0	116.7148	-9.40	112	0.12
Error	-	-	1.27%	2.86%	-	-

Table 1: Accuracy and efficiency for tetrachiral honeycomb.

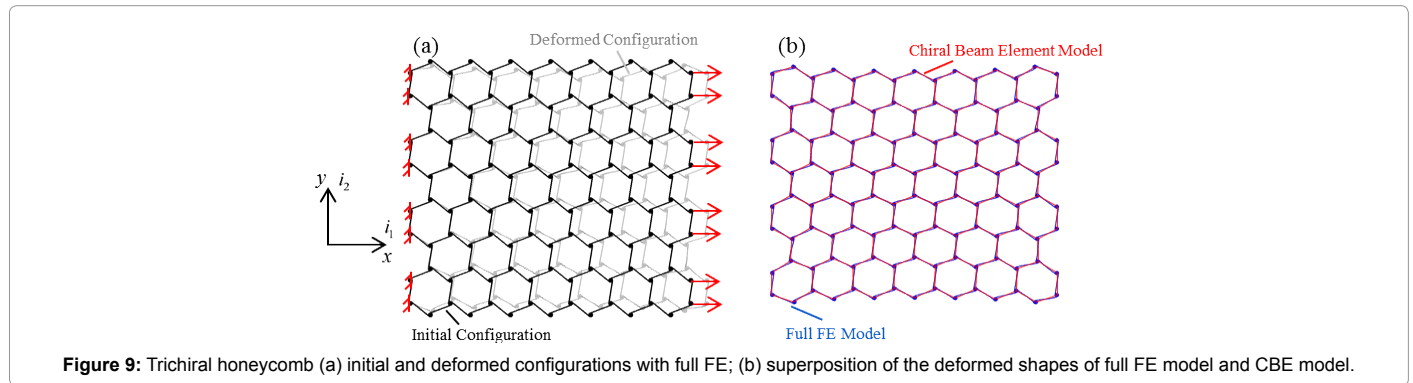


Figure 9: Trichiral honeycomb (a) initial and deformed configurations with full FE; (b) superposition of the deformed shapes of full FE model and CBE model.

Parameter	U1 (mm)	U2 (mm)	RF1 (N)	NOE	Time (s)
Full-FE	10	0	3.66	463189	167.76
CBE	10	0	3.82	165	0.14
Error	-	-	4.50%	-	-

Table 2: Accuracy and efficiency for trichiral honeycomb.

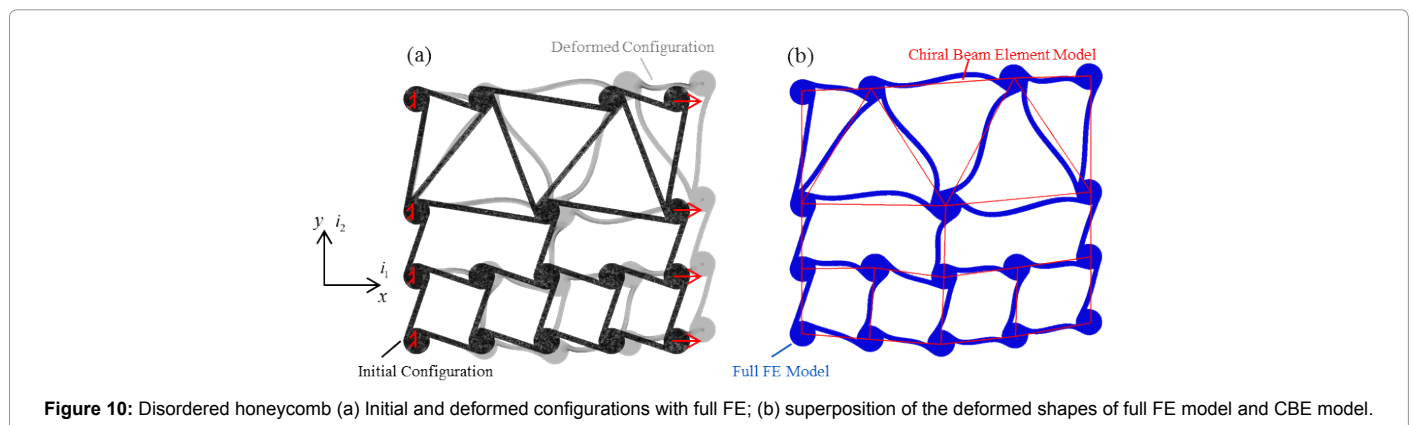


Figure 10: Disordered honeycomb (a) Initial and deformed configurations with full FE; (b) superposition of the deformed shapes of full FE model and CBE model.

$$error_{RF} = \left| \frac{RF_{full} - RF_{CBE}}{RF_{full}} \right| \quad (30)$$

As recorded in Table 1, the errors of reaction forces for CBE model are less than 3%. Adopting this user-defined element simplifies the modelling process and the number of required elements (NOE) is reduced. Compared with the full FE model, the computational time is decreased by over three orders of magnitude from 158.7s to 0.12s. In such case, both accuracy and efficiency is achieved by employing the user-defined CBE.

### Trichiral Chiral Honeycomb

In Figure 9, a trichiral honeycomb is studied. Similar to the previous case, the deformed shapes of two different models fit very well. The efficiency is improved and simplification of modelling can be expected as well. Although the global error increases a bit to 4.5% (Table 2), it is still acceptable.

### Disordered Chiral Honeycomb

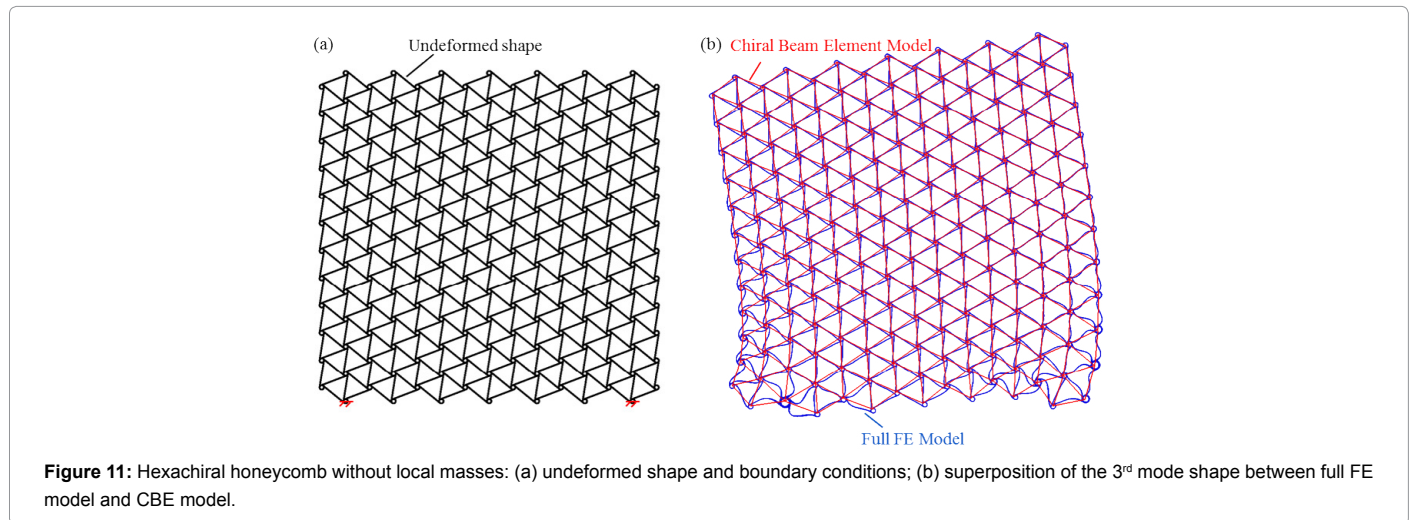
As shown in Figure 10, the most attractive advantage of this CBE is that it can model these disordered chiral honeycombs conveniently. It is known that RVE cannot be adopted to analyze the irregular structure and hence the full FE model should be utilized, which is tedious and time-consuming. However, adopting the CBE, significant simplification of the modelling can be achieved. Free end tension ( $U1=10$  mm,  $U2$  free) is imposed on the structure, as shown in Figure 10a. It can be found from Figure 10b and Table 3 that satisfactory agreement and accuracy are obtained. As can be expected, if large and disordered chiral honeycombs are considered, the superiority of the CBE model will be more dominant.

### Dynamic analyses

The chiral honeycomb structures may consist of different materials for specific designing targets [12]. The honeycombs could be plastic while the local masses could be metal (Figure 6). As shown in Eq. (27-

Parameter	U1 (mm)	U2 (mm)	RF1 (N)	NOE	Time (s)
Full-FE	10	4.9762	299.2671	52112	46.08
CBE	10	4.7287	312.3904	27	0.12
Error	-	4.97%	4.39%	-	-

Table 3: Accuracy and efficiency for disordered honeycomb.



Mode	1	2	3	4	5	NOE	Time (s)
Full-FE (Frequency)	21.26	37.45	45.13	87.90	105.88	997654	1732.1
CBE (Frequency)	22.35	39.38	46.93	90.49	110.46	508	0.43
Error	5.13%	5.15%	4.00%	2.95%	4.33%	-	-

Table 4: Frequency of different modes and the error between full FE model and CBE model for honeycomb without local masses.

29), the mass of different components can be assigned independently when we construct the mass matrix of the CBE.

The same geometric and elastic properties for the CBE are adopted as in section 3.1. According to Figure 6, the density of honeycomb material (nodes and ligaments) is set to be 1500 kg/m<sup>3</sup> while the density of local internal masses is 8050 kg/m<sup>3</sup>. If pure honeycombs are analyzed [17], local masses are not present and the density of the local masses is 0 accordingly. In this section, the modal analysis is performed on the honeycomb structures and the mode shapes as well as the frequencies are measured.

### Honeycomb without Local Masses

Setting the local mass to be zero, the pure honeycomb structure will be obtained. As shown in Figure 11a, two nodes at the bottom are fixed and the frequency analysis is conducted. Figure 11b shows the 3<sup>rd</sup> mode shapes obtained from both full FE and CBE model. It can be observed that the mode shapes and mode frequencies can be well predicted by the simplified CBE model. Furthermore, the computational time (analysis for the first 20 modes) drops to a great extent from 1732.1s to 0.43s, as shown in Table 4.

### Honeycomb with Local Masses

As shown in Figure 12a, the local masses (red shaded) are inserted in the hollow nodes of the honeycomb structure. This structure can be applied to control and mitigate the vibrations [12]. Similar analysis is conducted and the results are shown in Figure 12b and Table 5. The errors in predicting the modal frequencies for this case are quite small, generally below 0.5% for the first 5 modes, which is negligible.

To conclude, from all the examples shown above, it should be noted that if the big and complicated honeycombs are analyzed, the CBE models can save huge amount of computational time compared to the full FE models. The computational time of CBE element models is always less than 1 second while, for the full FE models, it can go up to over one thousand seconds. In addition, the errors brought about by applying this CBE are generally below 5%, which are small and acceptable.

### Conclusions

In this paper, a user-defined CBE is established in order to replace the traditional FE when modelling the chiral honeycombs. The detailed construction and modelling procedures are illustrated. By simply connecting the center points with CBEs, dramatic simplification is achieved compared with the full FE modelling. Several numerical examples are given over a range of configurations and satisfactory agreements are obtained. Applying this CBE, the computational time can be reduced by several orders of magnitude if honeycombs with large structures are analyzed. Overall, the CBE proposed in this paper provides a simple and effective method to model the chiral honeycombs.

### Acknowledgement

The first author greatly acknowledges the research scholarship and research grant ( No. R265000523646 ) from National University of Singapore.

### References

- Alderson A, Alderson K, Attard D, Evans K, Gatt R, et al. (2010) Elastic constants of 3-, 4-and 6-connected chiral and anti-chiral honeycombs subject to uniaxial in-plane loading. *Compos Sci Technol* 70: 1042-1048.
- Prall D, Lakes R (1997) Properties of a chiral honeycomb with a Poisson's ratio of 1. *Int J Mech Sci* 39: 305-314.

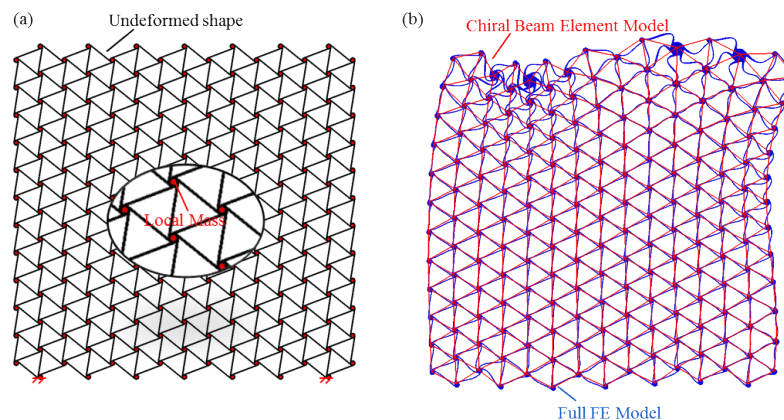


**Figure 12:** Hexachiral honeycomb local masses: (a) undeformed shape and boundary conditions; (b) superposition of the 8<sup>th</sup> mode shape between full FE model and CBE model.

Mode	1	2	3	4	5	NOE	Time (s)
Full-FE (Frequency)	18.17	32.06	37.80	71.39	88.22	1112859	1841.6
CBE (Frequency)	18.09	31.92	37.70	71.61	88.61	508	0.32
Error	0.44%	0.44%	0.26%	0.31%	0.44%	-	-

**Table 5:** Frequency of different modes and the error between full FE model and CBE model for honeycomb with local masses.

- Grima JN, Gatt R, Farrugia PS (2008) On the properties of auxetic meta-tetrachiral structures. *Phys Status Solidi B* 245: 511-520.
- Hassan M, Scarpa F, Mohamed N, Ruzzene M (2008) Tensile properties of shape memory alloy chiral honeycombs. *Phys Status Solidi B* 245: 2440-2444.
- Lorato A, Innocenti P, Scarpa F, Alderson A, Alderson K, et al. (2010) The transverse elastic properties of chiral honeycombs. *Compos Sci Technol* 70: 1057-1063.
- Dirrenberger J, Forest S, Jeulin D (2013) Effective elastic properties of auxetic microstructures: anisotropy and structural applications. *Int J Mech Mater Des* 9: 21-33.
- Bacigalupo A, De Bellis ML (2015) Auxetic anti-tetrachiral materials: equivalent elastic properties and frequency band-gaps. *Compos Struct* 131: 530-544.
- Airoidi A, Bettini P, Panichelli P, Oktem MF, Sala G (2015) Chiral topologies for composite morphing structures—Part I: Development of a chiral rib for deformable airfoils. *Phys Status Solidi B* 252: 1435-1445.
- Airoidi A, Bettini P, Panichelli P, Sala G (2015) Chiral topologies for composite morphing structures—Part II: Novel configurations and technological processes. *Phys Status Solidi B* 252: 1446-1454.
- Hassan MR, Scarpa F, Ruzzene M, Mohammed N (2008) Smart shape memory alloy chiral honeycomb. *Mater Sci Eng A* 481: 654-657.
- Zhu R, Liu X, Hu G, Sun C, Huang G (2014) A chiral elastic metamaterial beam for broadband vibration suppression. *J Sound Vib* 333: 2759-2773.
- Baravelli E, Ruzzene M (2013) Internally resonating lattices for bandgap generation and low-frequency vibration control. *J Sound Vib* 332: 6562-6579.
- Spadoni A, Ruzzene M (2006) Structural and acoustic behavior of chiral truss-core beams. *J Vib Acous* 128: 616-626.
- Bacigalupo A, Gambarotta L (2016) Simplified modelling of chiral lattice materials with local resonators. *Int J Solids Struct* 83: 126-141.
- Kumar RS, McDowell DL (2004) Generalized continuum modeling of 2-D periodic cellular solids. *Int J Solids Struct* 41: 7399-7422.
- Spadoni A, Ruzzene M (2012) Elasto-static micropolar behavior of a chiral auxetic lattice. *J Mech Phys Solids* 60: 156-171.
- Tee K, Spadoni A, Scarpa F, Ruzzene M (2010) Wave propagation in auxetic tetrachiral honeycombs. *J Vib Acous* 132: 031007.
- Scarpa F, Blain S, Lew T, Perrott D, Ruzzene M, et al. (2007) Elastic buckling of hexagonal chiral cell honeycombs. *Composites: Part A* 38: 280-289.
- Bacigalupo A, Gambarotta L (2014) Homogenization of periodic hexa-and tetrachiral cellular solids. *Compos Struct* 116: 461-476.
- Jacobs S, Coconnier C, DiMaio D, Scarpa F, Toso M (2012) Deployable auxetic shape memory alloy cellular antenna demonstrator: design, manufacturing and modal testing. *Smart Mater Struct* 21: 7.
- Liu X, Huang G, Hu G (2012) Chiral effect in plane isotropic micropolar elasticity and its application to chiral lattices. *J Mech Phys Solids* 60: 1907-1921.
- Chen Y, Scarpa F, Liu Y, Leng J (2013) Elasticity of anti-tetrachiral anisotropic lattices. *Int J Solids Struct* 50: 996-1004.
- Liu GR, Quek SS (2013) *The finite element method: A practical course*. Butterworth-Heinemann, UK.